Available online at www.sciencedirect.com
ScienceDirect
Journal of Power Sources 175 (2008) 903–908
JOURNAL OF POWER SOURCES
www.elsevier.com/locate/jpowsour

Short communication

Preparation and electrochemical properties of carbon-doped TiO_2 nanotubes as an anode material for lithium-ion batteries

Jinwei Xu, Yunfei Wang, Zonghui Li, W.F. Zhang *

School of Physics & Electronics, Henan University, Kaifeng 475001, PR China

Received 11 May 2007; received in revised form 19 September 2007; accepted 6 October 2007
Available online 11 October 2007

Abstract

Carbon-doped TiO_2 nanotubes were synthesized through a sol–gel and subsequent hydrothermal process. Transmission electron microscopy and X-ray diffraction showed that the products are uniformly straight tubes with the diameter around 10 nm in anatase-type. The electrochemical performances of the nanotubes were tested by constant current discharge/charge, cyclic voltammetry, and electrochemical impedance spectroscopy. The initial discharge capacity reaches 291.7 mAh g^{-1} with a coulombic efficiency of 91.7% at a current density of 70 mA g^{-1}. There is a distinct potential plateau near 1.75 and 1.89 V (versus Li^+/Li) in the lithium intercalation and extraction processes, respectively, and the lithium insertion capacity is about 204 mAh g^{-1} over the plateau of 1.75 V region in the first cycle. From the 2nd to the 30th cycles, the average reversible capacity loss is less than 1.73 mAh g^{-1} per cycle. After 30 cycles, the reversible capacity still remains 211 mAh g^{-1} with a coulombic efficiency larger than 99.7%, implying a perfect reversibility and cycling stability.

Keywords: Carbon-doped TiO_2; Nanotube; Discharge; Capacity; Plateau

1. Introduction

In fine and portable electronic devices such as mobile telephone and watches, Li-ion batteries are excellent power sources because of their high energy storage density, long cycle life, little memory effect, poisonous-metals free, and so on. In present commercial lithium-ion batteries, graphite is widely used as an anode material, and $LiCoO_x$, $LiMnO_x$, or $LiNiO_x$ as cathode. However, the graphite anode has some disadvantages such as electrical disconnection, structural deformation, and initial loss of capacity [1], which dissatisfy the need of production. To avoid these drawbacks, transition metal oxides such as WO_3, MoO_3 and TiO_2 have attracted much attention [2–4]. Especially, titanium oxide is regarded as a promising active lithium intercalation material with high capacity, low-voltage (below ca. 2.0 V versus Li^+/Li) for lithium intercalation, and low production cost. In the structure of titanium oxide, the TiO_6 octahedra share vertices and edges to build up the three-dimensional framework, leaving favorable empty sites available for lithium insertion [5]. TiO_2 has various crystal types such as anatase, rutile, brookite, TiO_2(B), etc. [6–9]. Under standard conditions, rutile is the thermodynamically most stable structure of TiO_2, and is also the most common natural form. TiO_2(B) is a metastable monoclinic modification of titanium dioxide. Anatase is generally considered to be the most electroactive Li-insertion host among these TiO_2 polymorphs. However, rutile and TiO_2(B) for electrochemical Li insertion also aroused increasing interests [9–12]. For the micrometer-sized rutile, only a small degree of Li insertion (0.1–0.25 mol) can be observed; these values are typical for micrometer-sized rutile [10–12]. Li-insertion electrochemistry of microfibrous TiO_2(B) was recently reported and found to be basically different from that of anatase. The kinetics of lithium storage in anatase is controlled by solid-state diffusion of Li^+, whereas Li-insertion into TiO_2(B) is governed by a pseudocapacitive faradaic process [9].

In recent years, nanostructured materials for anode of lithium-ion batteries stimulated great interest since they demonstrated excellent improvement in the electrochemical properties than that of the respective micrometer materials. Nanostructured TiO_2 has been widely investigated as a key material for fun-

* Corresponding author. Tel.: +86 378 3881 940; fax: +86 378 3880 659.
E-mail address: wfzhang@henu.edu.cn (W.F. Zhang).

0378-7753/$ – see front matter © 2007 Elsevier B.V. All rights reserved.
doi:10.1016/j.jpowsour.2007.10.014

damental research and technological applications in the fields of optical devices, photovoltaic cells, photocatalysts, gas sensing, and electrochemical storage [13–16]. Especially, much attention has been paid to nanostructured TiO_2 for Li insertion, because it is not only a low-voltage insertion host for Li, but also a fast Li insertion/extraction host. These characteristics render it a potential anode material for high-power lithium-ion batteries, avoiding the necessity of a passivation layer at the contact to the liquid electrolyte [7,8,10]. Besides nanometer-sized anatase, the electrochemical performance of nanometer-sized rutile was also investigated [10], which showed surprising advantages compared with micrometer-sized rutile and was able to reversibly accommodate Li up to $Li_{0.5}TiO_2$ with excellent capacity retention and high-rate capability on cycling. Zhou et al. [17] and Li et al. [18] synthesized titanium oxide nanotubes and tested their electrochemical properties, respectively. Although they obtained different discharge/charge capacity, the discharge/charge voltage curves acquired by them kept sloping profiles with slight voltage plateaus, indicating that there were still some distances for their practical application. Recently, carbon-doped TiO_2 was prepared and attracted great interest as photocatalyst, and showed better photocatalytic activity [15,16]. However, to our knowledge, there is little report about the electrochemical performance of carbon-doped TiO_2. In the present paper, carbon-doped TiO_2 nanotubes were synthesized and the electrochemical performances were tested through constant current discharge/charge, cyclic voltammetry and electrochemical impedance spectroscopy.

2. Experimental

Carbon-doped TiO_2 nanotubes were prepared by two steps. Firstly, carbon-doped (nominally 2%) TiO_2 powders were synthesized using a sol–gel method as follows. Ten milliliters of $Ti(OC_4H_9)_4$ was dissolved in 40 mL ethanol to get solution (I). 10 mL H_2O, 2 mL HNO_3, 10 mL ethanol and 0.5 mL CCl_4 were mixed to get solution (II). Then, the solution (I) was slowly dropped into the solution (II) under constantly stirring to get the sol. After standing quietly for 6 h, the sol was dried at 70 °C for 36 h, and then calcined at 700 °C for 2 h. Secondly, the as-prepared carbon-doped TiO_2 powders were mixed with an aqueous 10 mol L^{-1} NaOH solution. After stirring for 1 h, the resulting suspension was transferred into a stainless-steel autoclave, then the autoclave was heated to 120 °C and maintained for 24 h. After cooling to room temperature naturally, the precipitates were rinsed with deionized water, neutralized with 0.1 mol L^{-1} HNO_3 solution and then washed with deionized water again until a pH value of about 7 was reached. Finally, after drying, the product was annealed at 500 °C for 2 h in air to get the sample. Undoped TiO_2 nanotubes were also fabricated through the similar route for comparison.

Transmission electron microscopy (TEM) images were taken with a JEOL JEM 100 CX-II instrument (Japan). X-ray diffraction (XRD) was performed on a DX-2500 diffractometer (China) with Cu Kα radiation operating at 40 kV and 25 mA. The 2θ range used in the measurement was from 20° to 60°. The diffuse reflectance spectra were recorded on an ultraviolet–visible (UV–vis) spectrometer (Varian Carry 5000) with $BaSO_4$ as the reference standard and were converted to the absorbance data through the Kubelka–Munk method.

The working electrode was prepared using mixture of 85 wt% active materials, 10 wt% acetylene black, and 5 wt% polyvinylidene fluoride binder. An organic solvent 1-methyl-2-pyrrolidone was dropped into the mixture to get slurry. The prepared slurry was homogenized by stirring and then uniformly coated on copper foil. After drying, the electrode films were pressed to provide increased adherence of the active material onto the copper foil current collector, and make the electrode materials compact. The cells consisted of the as-prepared electrode, lithium metal as the counter and reference electrode, and an electrolyte of 1.0 M $LiPF_6$ dissolved in a mixture of EC (ethylene carbonate) and DMC (dimethyl carbonate) with the volume ration of 1:1. A Celgard 2400 membrane was used as the cell separator. The cells were constructed in an Ar-filled glove box. The discharge/charge characteristic was measured using LAND Celltest (Wuhan, China) at a constant current density of 70 mA g^{-1} with cutoff voltages of 2.7–1.0 V. Cyclic voltammetry and alternating current (ac) impedance were performed on a CHI660B electrochemical work station. Cyclic voltammetry was recorded in the voltage range from 2.7 to 1.0 V at different scan rates of 0.5, 1.0 and 2.0 mV s^{-1}. The electrochemical impedance measurements were carried out by applying an ac voltage of 5 mV in the frequency from 100 kHz to 0.01 Hz. The current density and specific capacity were calculated based on the mass of the active material in the working electrode. All the electrochemical measurements were carried out using three-electrode system at room temperature.

3. Results and discussion

3.1. Characteristics of samples

Fig. 1 shows the TEM images of carbon-doped TiO_2 nanotubes. It can be seen that the products are long slim tubular shape, whose diameter is around 10 nm and length is several

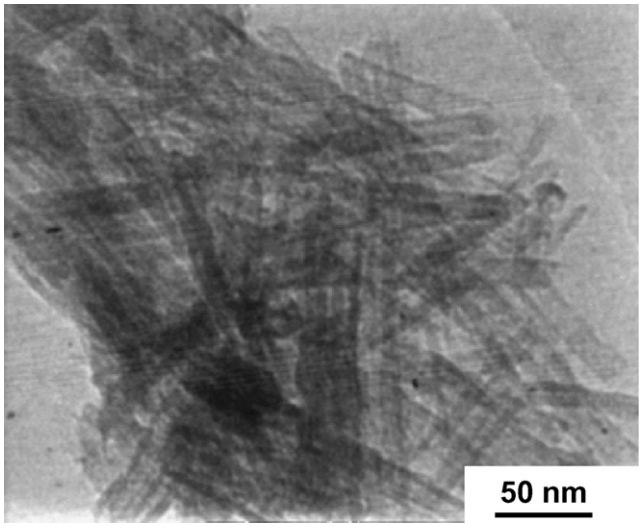

Fig. 1. TEM image of the as-prepared carbon-doped TiO_2 nanotubes.

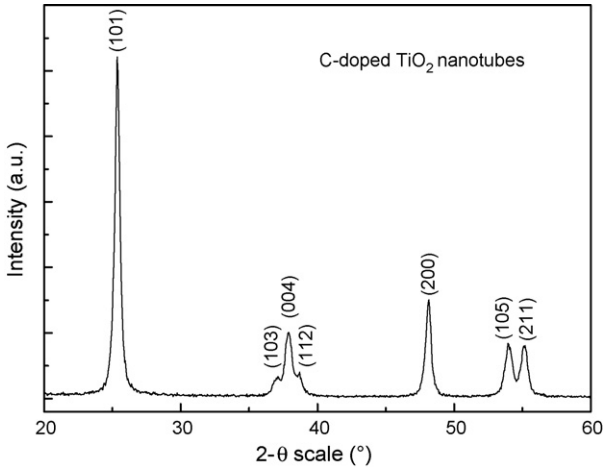

Fig. 2. XRD patterns of the as-prepared carbon-doped TiO_2 nanotubes.

hundred nanometer. The XRD pattern of carbon-doped TiO_2 nanotubes is shown in Fig. 2. All diffraction peaks can be indexed as anatase, without any other phases. The intense peaks indicate that the TiO_2 nanotubes are well crystallized. Usually, anion doping obviously influences light absorption features of TiO_2 [19–21]. Fig. 3 shows the UV–vis absorption spectra of the undoped (white) and carbon-doped TiO_2 (slightly yellow) nanotubes. A significant increase in the absorption at wavelengths shorter than 400 nm can be assigned to the intrinsic band-gap absorption of TiO_2 [19]. The absorption spectrum of the carbon-doped TiO_2 shows a stronger absorption in the UV–vis region and a red shift in the absorption edge. The red shift is attributed to the fact that carbon doping can narrow the band-gap of the TiO_2 by the mixing the O 2p orbits with C 2p orbits [21]. These results reveal that the carbon is indeed incorporated into the lattice of TiO_2 [22].

3.2. Electrochemical behavior of samples

Fig. 4 displays the initial six discharge/charge curves of carbon-doped TiO_2 nanotubes electrode between the cutoff voltages from 2.7 to 1.0 V (versus Li^+/Li) at a current density of 70 mA g^{-1}. During the first discharge process, the voltage decreases rapidly to 1.78 V, and then attains a plateau of about 1.75 V. The discharge capacity in this voltage plateau region is around 204 mAh g^{-1}, which occupies about 70% of the entire discharge capacity, revealing that the potential can keep stable for a long period of time during discharge. The discharge/charge capacity reaches as high as 291.7 and 267.4 mAh g^{-1} with a coulombic efficiency of 91.7% in the first cycle. In the second cycle, there is a comparatively large discharge capacity decrease of about 19.1 mAh g^{-1}. After a significant capacity drop (the average discharge capacity loss is about 12.2 mAh g^{-1} per cycle) in the initial four cycles, from the fourth to the sixth cycle, the average capacity loss is smaller. During the process of constant current discharge and charge, long voltage plateaus near/at 1.75 and 1.89 V for discharging (insertion of lithium) and charging (extracting of lithium) can be seen clearly, respectively, which is consistent with the presence of predominant anatase as the starting materials [4,23]. The flat voltage plateau is characteristic of a two-phase electrochemical reaction [24], and the lithium insertion proceeds through a two-phase equilibrium of a Li-poor and a Li-rich phase [25]. The wide potential plateaus also indicate that the insertion and extraction of lithium ions occur in one stage [26]. In addition, at the end of discharge/charge voltage plateaus the potential decreases or increases quickly, which can be used as an indication of the end of discharge/charge [24]. By comparison, the first discharge/charge curves of undoped TiO_2 nanotubes electrode are given in Fig. 4 (dashed lines). As shown, in case of undoped TiO_2 nanotubes electrode, the discharge voltage curve shows a sloping profile, and the voltage plateau is shorter and becomes indistinct. A large part of the discharge capacity is due to the long sloped-region from 1.7 to 1.0 V. Although the first discharge capacity reaches 278 mAh g^{-1}, there is a higher irreversible capacity, which is about 60 mAh g^{-1}. The result shows that the dopant of carbon not only prolongs the discharge/charge voltage plateaus but also minimizes the first irreversible capacity loss efficiently.

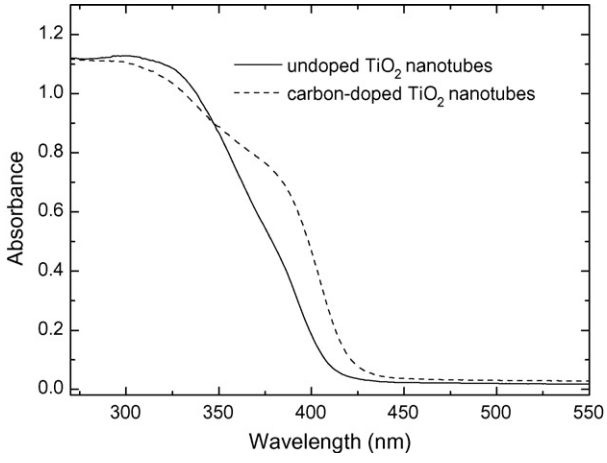

Fig. 3. UV–vis absorption spectra for undoped and carbon-doped TiO_2 nanotubes annealed at 500 °C for 2 h.

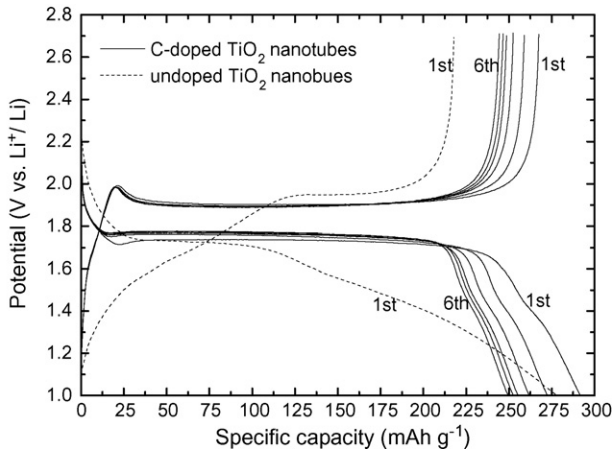

Fig. 4. The initial six discharge/charge curves of the carbon-doped TiO_2 nanotube electrode and the first discharge/charge curve of the undoped TiO_2 nanotube electrode.

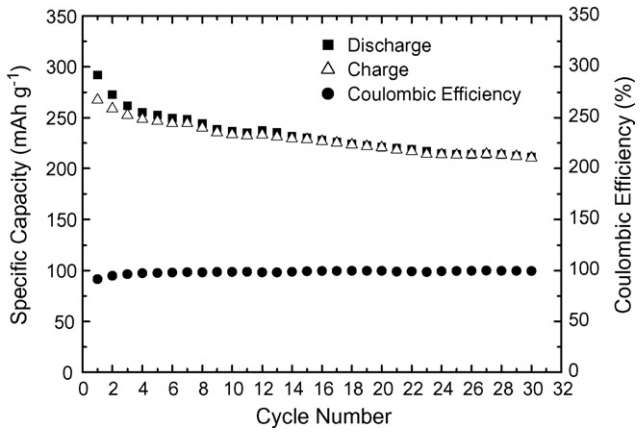

Fig. 5. Cycling performance of the carbon-doped TiO_2 nanotube electrode.

Fig. 5shows the cycling performance of the nanostructure electrode at a current density of 70 mA g^{-1} between 2.7 and 1.0 V. In the first cycle, the irreversible capacity is about 24.3 mAh g^{-1} and the coulombic efficiency reaches 91.7%. For the TiO_2 anode, this small irreversible loss of capacity on the first cycle is not associated with a solid electrolyte interface (SEI) layer formation [27]. During discharge/charge cycles, the potential was confined above 1.0 V, this should minimize electrolyte reduction and hence any SEI layer formation. The irreversible lithium intercalation capacity in the first cycle can be ascribed to lithium intercalation into irreversible sites and side reaction arising from trace water absorbed because of the large specific area of nanotubes [18]. The irreversible Li-insertion sites are almost filled completely and trace water is consumed gradually during the initial several cycles, so the discharging/charging tends to stabilization in the following cycles. There are other explanations for the irreversible capacity loss es, for example, it may be due to the poor intrinsic electronic conductivity of the electrode, on recharge, the region near the surface becomes depleted of $Li^+ + e^-$ may result in poor electronic conductivity and hence significant polarization, such that the remaining Li is not easily removed [27,28]. The discharge/charge capacity is 272.6 and 258.9 mAh g^{-1}, respectively, and the coulombic efficiency is about 95% in the second cycle. From the 2nd to the 30th cycle, the average reversible capacity loss is less than 1.73 mAh g^{-1} per cycle and the coulombic efficiency increases gradually. After 30 cycles, the reversible capacity still keeps 211 mAh g^{-1} with a coulombic efficiency larger than 99.7%. For TiO_2 electrode, the structure instability during lithium intercalation and de-intercalation gives rise to rapid capacity fading [29,30]. The excellent cycling stability and perfect reversibility of carbon-doped TiO_2 nanotubes electrode, indicates that there is no significant structure change occurring when lithium inserting and extracting. This may be attributed to the dopant of carbon, which can suppress the structure degradation of electrode material during the lithium insertion/extraction process and also improve the conductivity of the electrode. On the other hand, the large specific surface area of nanotubes material can relieve the stress associated with the volume changes more easily in the process of lithium intercalation/extraction, increase the electrode–electrolyte contact area, and decrease the specific current density of the active material.

Cyclic voltammetry patterns were recorded from 2.7 to 1.0 V (versus Li^+/Li) at different scan rates after 10 discharge/charge cycles, so as to minimize the influence of side reaction coming from trace water. Obviously, with the scan rate increasing, both the peak separation and the peak current increase synchronously. Generally, the peak potential is associated with the scan rate, since at larger scan rate the systems may yield irreversibility, and the cathodic/anodic peaks will shift to lower/higher potentials, respectively. As shown in Fig. 6, when a scan rate of 0.5 mV s^{-1} is applied, in each cycle there is only a single pair of sharp cathodic/anodic peaks located at 1.59 and 2.2 V (the actual peak potentials depend on the scan rate) with poorly defined shoulders, which may reflect mainly the capacity effects [31]. This pair of peaks is in accordance with the plateaus of the discharge/charge curves. It is clear that the integral charge in the cathodic/anodic branch approaches, and the ratio of cathodic/anodic peak currents is nearly 1, demonstrating an excellent reversibility. As expected, it exhibited a small irreversible capacity and relatively little difference between the first and the second cycles. It is also found that the peak current at different scan rates is in proportion to square-root of the scan rate, $v^{1/2}$, indicating that the reaction kinetics is controlled by the diffusion step [32,33]. The behavior described by i–$v^{1/2}$ is typical for Li-insertion into ordinary anatase lattice. It should be noted that microfibrous TiO_2(B) does not follow the square-root dependence. This is because that Li-insertion into TiO_2(B) is governed by a pseudocapacitive faradaic process [9] other than solid-state diffusion of Li^+. No S-peaks were observed in Fig. 6, which show that they are pure anatase nanotubes. This is in accord with the XRD pattern and TEM image of the prepared materials. The CV curves also imply that this electrode possesses excellent cycling stability and reversibility, in agreement with the result of the cycling performance shown in Fig. 5.

ac impedance spectroscopy is a powerful technique to determine the kinetic parameters of the electrode process [34,35]. The ac impedance spectrums of carbon-doped and undoped TiO_2

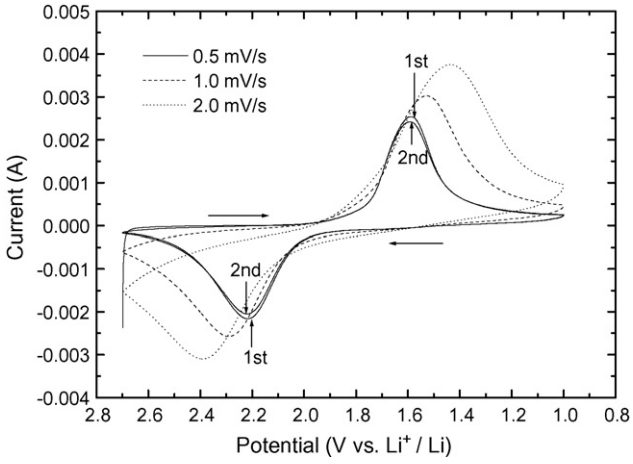

Fig. 6. Cyclic voltammogram plots of the carbon-doped TiO_2 nanotube electrodes at different scan rate of 0.5, 1.0 and 2.0 mV s^{-1}.

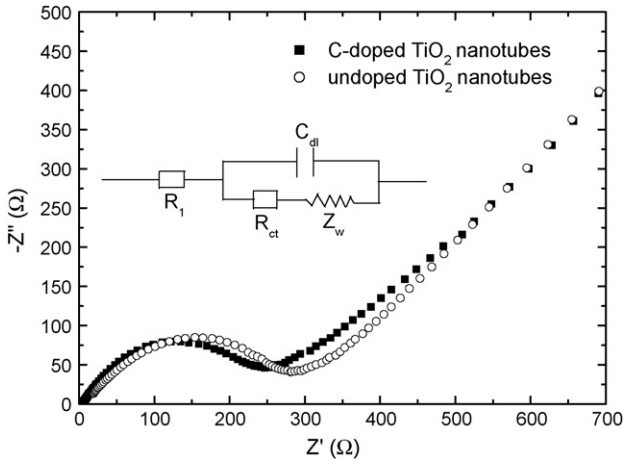

Fig. 7. Electrochemical impedance spectra of the carbon-doped and undoped TiO_2 nanotube electrodes.

nanotubes electrodes are illustrated in Fig. 7. As can be seen, both the Nyquist plots are characteristic of one semicircle in the high frequency range and a sloping straight line in the low frequency range, and only one semicircle is observed in the high frequency range, which may be consistent with the absence of a SEI layer on the electrode surface. The semicircle in high frequency range represents an electrochemistry-controlled process, relating to the charge transfer through the electrode/electrolyte interface. The inclined straight line in low frequency range represents a diffusion-controlled process, namely, reflects the solid-state diffusion of Li-ions in the electrode materials. From the ac impedance spectrum, a typical equivalent circuit was depicted in the inset of Fig. 7, where R_1 is the ohmic resistance of the electrolyte, membrane and electrode, corresponding to the high frequency intercept of the semicircle with the horizontal axis, C_{dl} and R_{ct} represent the double-layer capacitance and the charge-transfer resistance, respectively, corresponding to the semicircle, and Z_w is the Warburg impedance arising from the semi-infinite diffusion of Li^+ ions in electrode, corresponding to the inclined straight line in low frequency. From the Nyquist plots, it can be found that both R_1 and the size of the semicircle of carbon-doped TiO_2 nanotubes electrode are smaller than those of undoped TiO_2 nanotubes electrode, respectively, which indicates that the resistance of carbon-doped TiO_2 nanotubes electrode is reduced by increasing the conductivity, and the charge-transfer resistance (R_{ct}) of carbon-doped TiO_2 nanotubes electrode is smaller than that of undoped TiO_2 nanotubes electrode, it may be ascribed to the dopant of carbon in the TiO_2 nanotubes.

4. Conclusions

Slim long carbon-doped TiO_2 nanotubes with a diameter of about 10 nm and length of several hundred nanometers were synthesized via sol–gel method and subsequent hydrothermal process. XRD shows that the products crystallized in anatase. The electrode delivers a lithium intercalation specific capacity of 291.7 mAh g^{-1} and the corresponding extraction capacity is 267.4 mAh g^{-1} with a coulombic efficiency of 91.7% at a current density of 70 mA g^{-1} in the first cycle. The reversible capacity maintains 211 mAh g^{-1} with a coulombic efficiency larger than 99.5% after 30 cycles, and the long voltage plateaus keep stable during discharge/charge. CV curves indicate that the lithium insertion into electrodes is a diffusion-controlled process. Comparing with undoped TiO_2 nanotubes electrode, the ohmic resistance and the charge-transfer resistance of carbon-doped TiO_2 nanotubes electrode are smaller. It is reasonable to think that carbon dopant plays an essential role in enhancing the electrochemical performances.

Acknowledgements

This work has been supported by National Natural Science Foundation of China (Grant No. 60476001) and by the Project of Cultivating Innovative Talents for Colleges & Universities of Henan Province (no. 2002006).

References

[1] K.M. Abrham, Electrochim. Acta 38 (1993) 1233.
[2] C. Natarajan, K. Setoguchi, G. Nogami, Electrochim. Acta 43 (1998) 3371.
[3] J.J. Auborn, Y.L. Barbero, J. Electrochem. Soc. 134 (1987) 368.
[4] S.Y. Huang, L. Kavan, I. Exnar, M. Grätzel, J. Electrochem. Soc. 142 (1995) L142.
[5] A. Kuhn, R. Amandi, F. García-Alvarado, J. Power Sources 92 (2001) 221.
[6] J.F. Banfield, D.R. Veblen, Am. Miner. 77 (1992) 545.
[7] L. Kavan, M. Grätzel, S.E. Gilbert, C. Klemenz, H.J. Scheel, J. Am. Chem. Soc. 118 (1996) 6716.
[8] I. Exnar, L. Kavan, S.Y. Huang, M. Grätzel, J. Power Sources 68 (1997) 720.
[9] M. Zukalová, M. Kalbáč, L. Kavan, I. Exnar, M. Grätzel, Chem. Mater. 17 (2005) 1248.
[10] Y.S. Hu, L. Kienle, Y.G. Guo, J. Maier, Adv. Mater. 18 (2006) 1421.
[11] W.J. Macklin, R.J. Neat, Solid State Ionics 53–56 (1992) 694.
[12] L. Kavan, D. Fattakhova, P. Krtil, J. Electrochem. Soc. 146 (1999) 1375.
[13] B. O'Regan, M. Grätzel, Nature 353 (1991) 737.
[14] G.K. Boschloo, A. Goossens, J. Schoonman, J. Electrochem. Soc. 144 (1997) 1311.
[15] Y. Li, D.S. Hwang, N.H. Lee, S.J. Kim, Chem. Phys. Lett. 404 (2005) 25.
[16] S.U.M. Khan, M. Al-Shahry, W.B. Ingler, Science 297 (2002) 2243.
[17] Y.K. Zhou, C. Lin, F.B. Zhang, B.L. He, H.L. Li, J. Electrochem. Soc. 150 (2003) A1246.
[18] J.R. Li, Z.L. Tang, Z.T. Zhang, Electrochem. Solid State Lett. 8 (2005) A316.
[19] R. Asahi, T. Morikawa, T. Ohwaki, K. Aoki, Y. Taga, Science 293 (2001) 269.
[20] J.S. Park, W. Choi, Langmuir 20 (2004) 11523.
[21] T. Tachikawa, S. Tojo, K. Kawai, M. Endo, M. Fujitsuka, T. Ohno, K. Nishijima, Z. Miyamoto, T. Majima, J. Phys. Chem. B 108 (2004) 19299.
[22] J. Yu, M. Zhou, B. Cheng, Z. Zhao, J. Mol. Catal. A 246 (2006) 176.
[23] A. Stashans, S. Lunell, R. Bergstrom, A. Hagfeldt, S.E. Lindquist, Phys. Rev. B 53 (1996) 159.
[24] A.N. Jansen, A.J. Kahaian, K.D. Kepler, P.A. Nelson, K. Amine, D.W. Dees, D.R. Vissers, M.M. Thackeray, J. Power Sources 81/82 (1999) 902.
[25] M.V. Koudriachova, N.M. Harrison, S.W. de Leeuw, Solid State Ionics 152/153 (2002) 189.
[26] B.L. He, B. Dong, H.L. Li, Electrochem. Commun. 9 (2007) 425.
[27] A.R. Armstrong, G. Armstrong, J. Canales, P.G. Bruce, J. Power Sources 146 (2005) 501.
[28] H. Huang, W.K. Zhang, X.P. Gan, C. Wang, L. Zhang, Mater. Lett. 61 (2007) 296.
[29] Y. Yagi, M. Hibino, T. Kudo, J. Electrochem. Soc. 144 (1997) 4208.

[30] L.D. Noailles, C.S. Johnson, J.T. Vanghey, M.M. Thackeray, J. Power Sources 81/82 (1999) 259.
[31] L. Kavan, M. Grätzel, L. Rathouský, A. Zukal, J. Electrochem. Soc. 143 (1996) 394.
[32] L.J. Fu, H. Liu, H.P. Zhang, C. Li, T. Zhang, Y.P. Wu, H.Q. Wu, J. Power Sources 159 (2006) 219.
[33] L. Kavan, M. Kalbáč, M. Zukalová, I. Exnar, V. Lorenzen, R. Nesper, M. Grätzel, Chem. Mater. 16 (2004) 477.
[34] G.X. Wang, D.H. Bradhurst, H.K. Liu, S.X. Dou, Solid State Ionics 120 (1999) 95.
[35] M. Mohamedi, D. Takahashi, T. Itoh, M. Umeda, I. Uchida, J. Electrochem. Soc. 149 (2002) A19.